https://doi.org/10.3311/PPci.41549

Periodica Polytechnica Civil Engineering, 69(4), pp. 1393–1408, 2025

Sustainable Utilization of Red Mud and Glass Waste in Alkali-Activated Cements: Design and Performance of Products

Adrienn Boros[1*], László Pintér[1], Tamás Korim[1]

[1] Department of Materials Engineering, Faculty of Engineering, University of Pannonia, H-8201 Veszprém, P.O.B. 158, Hungary
[*] Corresponding author, e-mail: boros.adrienn@mk.uni-pannon.hu

Received: 07 July 2025, Accepted: 12 November 2025, Published online: 24 November 2025

Abstract

Red mud (RM) is a hazardous waste that is generated in large quantities, and its sustainable, rational treatment and recovery is still a challenge. The aim of this research is to develop higher added value alkali-activated cements (AACs), which, by using red mud, can help to protect limited resources, reduce pollution, and produce alternative, "greener" building materials. During this work, industrial waste materials – blast furnace slag, red mud, and glass waste – were used to produce AACs suitable for traditional construction applications (e.g., load-bearing structures, foundation blocks, and walkways). Key parameters including the maximum RM content (recommended 21.7 wt% to maintain sufficient strength), composition of the activating solution, liquid/solid ratio, particle size, and reactivity of the glass waste were optimized. Glass waste reactivity was enhanced by high-energy grinding at 200 rpm for 90 minutes, resulting in a maximum compressive strength of 66.8 MPa, exceeding the highest strength class defined by relevant standards (EN 197-1). Mechanical properties were supported by microstructural analyses (SEM, FT-IR), and heavy metal behavior was assessed through leachate and adsorption tests. The AACs effectively immobilized heavy metals such as Cd, Ni, Pb, and Hg, with long-term leaching resistance and improved retention capacity compared to Portland cement-based mortars. Additionally, powder-based Pb^{2+} adsorption tests confirmed that RM-containing AACs offer enhanced performance in removing lead from aqueous solutions. Overall, these binders – containing up to 71.4 wt% combined industrial waste – demonstrate competitive mechanical and environmental properties, contributing to sustainable construction practices and potential wastewater treatment applications.

Keywords

alkali-activated cement, red mud, glass waste, secondary raw material recovery, sustainable building materials development

1 Introduction

The literature often refers to alkali-activated binders as the "sustainable cements of the future" [1–4]. Due to their excellent mechanical and chemical properties, they could compete with traditional binders in the construction, energy, chemical, transportation, and infrastructure industries [3, 5–7]. However, due to problems related to their production and economic efficiency, alkali-activated cements (AACs) are not expected to replace Portland cement-based binders in the full range of applications [8, 9]. Nevertheless, it is possible to produce materials that could be the future basis for sustainable building materials by using locally available raw materials and applying appropriate mix design and preparation parameters [1, 2, 4, 10].

One of the great advantages of AACs is the ability to form products of sufficient strength and desired shape using nearly any powdery materials, including many polluting industrial wastes (e.g., red mud and glass waste) [11–14]. Furthermore, certain industrial byproducts (e.g., blast furnace slag, fly ash, and silica fume) can serve as the basis for producing AACs [1, 15, 16]. Research is increasingly moving in this direction as waste continues to accumulate year after year, often without resolution. The same is true for red mud (RM), the storage of which is a worldwide problem [17–19]. Storing RM as a slurry requires a lot of land and carries a risk of dam failures. The safe disposal of dried red mud with reduced alkali content requires covered containers, since even the slightest gust of wind can pick up the fine particles [17, 18]. The Hungarian tailings dam failure (Ajka alumina plant) caused loss of human life, pollution of the environment, and invaluable economic and ecological damage [20, 21]. This industrial disaster has drawn attention to the fact that

Cite this article as: Boros, A., Pintér, L., Korim, T. "Sustainable Utilization of Red Mud and Glass Waste in Alkali-Activated Cements: Design and Performance of Products", Periodica Polytechnica Civil Engineering, 69(4), pp. 1393–1408, 2025. https://doi.org/10.3311/PPci.41549

storage only postpones the problem. Instead of continuing with disposal practices, it is essential to explore alternative uses of red mud that allow for the production of higher added-value products. The primary problem is that there are few economically viable solutions for the use of RM.

The recovery of red mud has been the subject of many studies from the very beginning. A significant part of such research includes metallurgical and metal recovery experiments, catalysis applications, and ceramics and building materials production [11, 12, 22–25]. However, despite all these advantages, these uses have not been widely adopted, primarily due to the highly alkaline chemistry of red mud [22, 25, 26]. The high pH corrodes iron-containing structural parts quickly, which makes the profitability of production questionable. When red mud is used in AACs, this problem does not occur; thus, this field offers promising opportunities [27–29]. While its use is beneficial from a sustainability point of view, we should not forget that there can be long-term drawbacks. When RM is used in large quantities, the high Fe_2O_3 content can slow down reaction kinetics; the excessive alkalinity can lead to gel instability and cracking; and the high fineness can increase shrinkage tendencies, which can ultimately result in a degradation of strength values [13, 30]. Furthermore, it is important to investigate whether the matrix can completely bind/immobilize the heavy metals in RM or if they can leach out over time [28, 31]. Combining red mud with more active raw materials (e.g., blast furnace slag) can help to avoid these difficulties [13, 30, 32]. Optimized material combinations have been shown to be essential for achieving favorable mechanical performance and long-term stability in red mud-based alkali-activated systems [33, 34]. These findings underline the importance of careful mix design and highlight the need for further research into long-term performance aspects such as heavy metal immobilization.

The properties of AACs can be influenced not only by the starting materials but also by the additives. In these systems, construction-grade quartz sand, which is becoming scarce globally [35, 36], can be replaced by recycled additives (e.g., construction and demolition waste, glass cullet, etc.) [14, 37]. Certain waste materials can serve as both recyclable aggregates and active components when finely ground [29, 38]. Glass waste (GW), for example, is reactive in an alkaline environment when used in a suitable particle size (<75 μm) [14, 29, 39, 40]. Due to its high silica content and amorphous nature, GW reacts with calcium sources present in the system to promote the formation of strength-providing C–S–H phases. This reactivity significantly improves the properties of the binder, such as strength, compactness, and chemical and fire resistance [14, 27, 32, 40].

The present study examines the potential production of AAC composites containing red mud. The work includes determining the maximum amount of red mud that can be incorporated into the matrix, examining the applicability of a given particle size fraction of glass waste as aggregate, and exploring ways to enhance the GW's reactivity through high-energy grinding. In addition to investigating the mechanical properties of AACs, the paper focuses on determining the heavy metal leaching and the adsorption capacity and on conducting a comparative experiment with traditional binders. The novelty of this research lies in the combined use of multiple industrial waste materials – red mud, ground glass waste, and granulated blast furnace slag – to develop AAC composites with improved mechanical and environmental performance. Unlike previous studies, the present work explores the direct utilization of untreated red mud and aims to optimize glass waste reactivity through particle size refinement. The proposed approach provides a feasible route to recycle hazardous industrial residues without the need for additional pre-treatment, while offering a sustainable alternative to conventional binders. As such, AAC composites based on waste materials may offer viable solutions not only for reducing the demand for natural raw materials but also for addressing waste management challenges, particularly in the production of load-bearing structural elements, foundation blocks, and walkways. To evaluate the performance and environmental characteristics of the developed AAC composites, compressive strength tests, heavy metal leaching measurements, and adsorption experiments were carried out.

2 Materials and methods

2.1. Materials

The raw materials used in the experiments were ground granulated blast furnace slag (GGBFS) and red mud powder (RM). The former was provided by ISD DUNAFERR Zrt. (Dunaújváros, Hungary), and the latter by MAL Magyar Alumínium Termelő és Kereskedelmi Zrt. (Ajka, Hungary). To enable comparative testing with traditional binders, specimens were prepared using CEM I 42.5 N type normal Portland cement (Duna-Dráva Cement Kft., Vác, Hungary).

Standard quartz sand (CEN Standard Sand according to EN 196-1 [41], Normensand GmbH, Beckum, Germany) was used as a filler for the preparation of AAC mortars. For the alternative aggregate mixtures, soda-lime glass waste (GW) (Guardian Orosháza Kft., Orosháza,

Hungary) was used instead. The maximum particle size of the standard quartz sand was 2 mm, while that of the glass waste was 1 mm. The glass waste was divided into fractions (1000–500, 500–250, 250–63, and 63–0 μm) with the help of sieve analysis. The fractionation was used to determine the reactivity of the GW, i.e., whether it acts as an inert material or an active component.

The chemical composition of the raw materials and GW (Table 1) was determined by X-ray fluorescence spectrometry (XRFS), the mineral composition by X-ray diffraction (XRD), and the amount of each phase by Rietveld analysis. Based on the XRD recording of the starting materials (Fig. 1), it can be concluded that the slag contains a significantly higher proportion of the amorphous phase (90.7 wt%) than the red mud (22.8 wt%). The GW is entirely amorphous.

In the case of GGBFS, merwinite (8.4 wt%) and akermanite (0.9 wt%) are identified as crystalline phases, while in the case of RM, the main crystalline phases are hematite (38.0 wt%) and cancrinite (11.8 wt%). The latter also contains minor amounts of quartz (5.7 wt%), goethite (5.6 wt%), larnite (5.5 wt%), magnetite (5.0 wt%), malladrite (3.0 wt%), and calcite (2.6 wt%).

Table 1 Chemical composition (wt%) of GGBFS, RM, and GW

Chemical composition (wt%)	GGBFS	RM	GW
SiO_2	38.96	14.58	71.82
Al_2O_3	6.70	18.51	2.18
CaO	41.19	12.43	4.84
MgO	8.28	0.49	3.37
Na_2O	0.46	13.27	16.76
K_2O	0.50	0.31	0.79
TiO_2	0.28	3.74	0.04
Fe_2O_3	0.41	32.89	0.17
SO_3	1.56	2.02	0.03
Loss on ignition	1.65	1.76	-

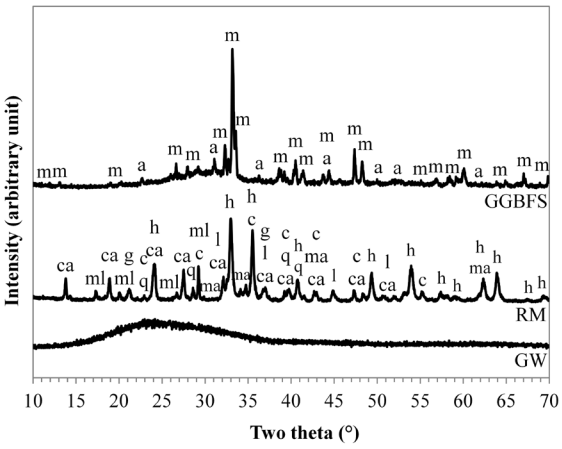

Fig. 1 XRD patterns of GGBFS, RM, GW (m: merwinite PDF 01-074-0382, a: akermanite PDF 01-087-0046, h: hematite PDF 01-089-0596, ca: cancrinite PDF 01-071-0776, q: quartz PDF 33-1161, g: goethite PDF 29-0713, l: larnite PDF 01-083-0461, ma: magnetite PDF 19-0629, ml: malladrite PDF 33-1280, c: calcite PDF 47-1743)

The particle size distribution of the raw materials and its median (D50) were determined by laser granulometry (Fig. 2): GGBFS: 21.3% < 5 μm, D50 = 19.3 μm, RM: 58.5% < 5 μm, D50 = 3.4 μm. The D50 value of the 63-0 μm GW fraction is 38.7 μm, with 9.8% of particles smaller than 5 μm. While D50 is not a direct measure of reactivity, it provides an indication of the fineness of the material, which is known to influence reactivity by affecting the available surface area for chemical reactions.

The activating solution used to prepare AACs was produced from a mixture of commercially available sodium silicate solution (ANDA Kft., Barcs, Hungary), analytical grade granular NaOH (Reanal Laborvegyszer Kereskedelmi Kft., Budapest, Hungary), and distilled water. The chemical composition of the sodium silicate solution (water glass) is as follows: 28.6 wt% SiO_2, 6.8 wt% Na_2O, and 64.6 wt% H_2O. The activating solution contained 9.35 wt% NaOH, 2.81 wt% Na_2O (from sodium silicate), 11.81 wt% SiO_2, and 76.0 wt% H_2O. Based on the estimated solution volume, the concentration of NaOH was 2.91 mol/L, or 4.05 mol/L when expressed as total NaOH equivalents including Na_2O.

Powder-based leaching experiments were performed using 99.8 wt% acetic acid (Lachner Ltd., Neratovice, Czech Republic) and 65 wt% nitric acid (Carlo Erba Reagents, Val-de-Reuil, France) solutions at standard concentrations. The former was used as the leaching solution (a dilution of

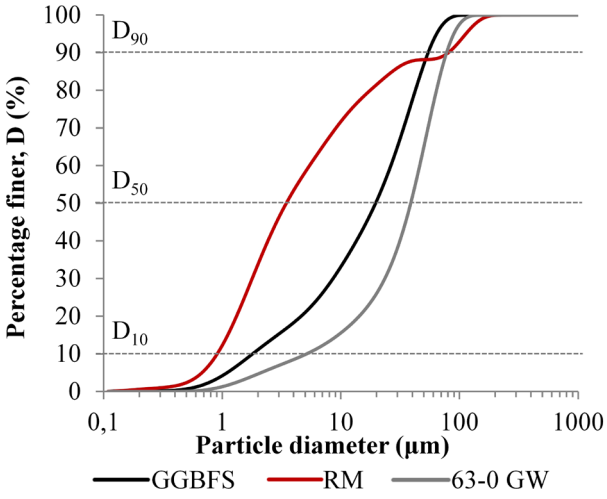

Fig. 2 Particle size distribution of GGBFS, RM, and GW (63-0 μm)

5.7 ml of acetic acid in 1 liter of distilled water, giving a pH of 2.88 ± 0.05), while the latter was used to adjust the pH to 1.3 ± 0.1 after the experiment. Nitric acid was also used to adjust the optimal pH of the solutions during the adsorption measurements. The 50 ppm Pb^{2+} solution used in the adsorption experiments was prepared using $PbCl_2$ (Sigma-Aldrich Chemie GmbH, Steinheim, Germany).

2.2 Sample preparation

During the experiments, the activating solution for the AAC mortar test specimens was prepared by dissolving solid sodium hydroxide (NaOH) directly in a mixture of sodium silicate solution (Na_2SiO_3) and distilled water. To ensure reproducibility, all mixtures were prepared using an activating solution that had been cooled to room temperature.

To prepare the samples, the required amount of GGBFS was first measured, followed by the addition of the room temperature activating solution. The mixing conditions were identical for all samples: the starting material/alkaline solution was homogenized for 45 seconds at 900 rpm, then the red mud, and finally the glass waste (or standard quartz sand for the control samples) was added. The resulting mortar was further mixed for 45-45 seconds at 900 rpm. The aggregate (standard quartz sand or glass waste) was added using a starting material (GGBFS + RM):aggregate mass ratio of 1:3.

The prepared mixture was cast into 30 × 30 mm cylindrical PVC molds and stored under ambient conditions (21-23 °C and RH = 50 ± 10%). Samples were demolded at 7 days of age, and qualification tests were performed at 7 and 28 days of age. Samples for the 28-day tests were stored under laboratory conditions at room temperature in the same way as before demolding.

In the first stage, GGBFS-based AAC samples were prepared using the following molar ratios: SiO_2/Al_2O_3 = 11.9, Na_2O/Al_2O_3 = 1.7, and the mass ratio of sodium silicate and sodium hydroxide in the activating solution was 4.4, and that of the activating solution and raw material (GGBFS + RM) was 0.7. It should be noted that this ratio refers only to the binder components. Taking into account the presence of inert quartz sand (at a binder-to-aggregate ratio of 1:3), the actual liquid-to-solid mass ratio of the complete mixture was 0.15. First, control samples were prepared using standard quartz and no red mud. Subsequently, mixtures with increasing red mud content were produced by partially replacing GGBFS with RM while maintaining a constant starting material-to-aggregate mass ratio (1:3). As the proportion of RM increased, the overall chemical composition of the binder changed accordingly. These changes are reflected in the calculated molar ratios of SiO_2/Al_2O_3 and Na_2O/Al_2O_3, which are summarized in Table 2. These ratios are crucial for understanding the chemical reactivity and gel formation potential of each mixture.

In the next step, the total amount of the aggregate in the mixture with the optimum red mud content (21.7 wt% by weight of GGBFS+RM) was replaced with glass waste of a given particle size range (1000-500, 500-250, 250-63, and 63-0 μm). Different liquid/solid (L/S) mass ratios (0.150, 0.188, 0.225, 0.263, 0.300, 0.350, 0.375) were used to determine the appropriate mixing consistency of the mixtures with each fraction. The increase of the liquid content of the mixtures was obtained by increasing the amount of activating solution. The mole ratios used were modified as shown in Table 3.

Further, the aim was to increase the strength of AAC mortars by increasing the reactivity of the glass waste used. For this purpose, the GW fraction between 500 and 250 μm was exposed to high-energy grinding. Firstly, the rotation speed was varied (150, 200, 250 rpm) using a constant grinding time (30 min), and then the grinding time was varied (30, 60, 90, 120 min) using 200 rpm. Samples were prepared from the resulting powders using a 0.350 L/S ratio. The molar ratios used were SiO_2/Al_2O_3 = 9.5, Na_2O/Al_2O_3 = 2.8. The composition of the activating solution was the same as in the previous sections, and the activating solution/(GGBFS+RM) mass ratio was 1.6.

In the final stage of the experiments, the relevant physical properties (strength, heavy metal leaching, and

Table 2 Experimental parameters for different red mud contents

	RM content by weight of GGBFS+RM, (wt%)					
	0.0	16.6	21.7	26.7	33.3	50.0
SiO_2/Al_2O_3 molar ratio	11.9	8.4	7.6	7.0	6.2	4.7
Na_2O/Al_2O_3 molar ratio	1.7	1.3	1.2	1.1	1.0	0.9

Table 3 Experimental parameters for different L/S ratios

L/S ratio	SiO_2/Al_2O_3 molar ratio	Na_2O/Al_2O_3 molar ratio	Activating solution / (GGBFS+RM) mass ratio
0.150	7.6	1.2	0.7
0.188	8.0	1.5	0.8
0.225	8.4	1.8	1.0
0.263	8.7	2.1	1.2
0.300	9.1	2.4	1.3
0.350	9.5	2.8	1.6
0.375	9.8	3.0	1.7

adsorption capacity) of the developed waste-based AAC were compared with the relevant values of one commercially available classical Portland cement (CEM I 42.5 N, in short: CEM I). The CEM I-based mortars were prepared using a cement-to-aggregate mass ratio of 1:3 and a water-to-cement ratio of 0.5. The size of the specimens was ø 30 × 30 mm. Since conventional binders are stored under water (as required by EN 12390-2 [42]), the storage conditions of the AAC composite samples were changed during the tests: room temperature laboratory atmosphere or underwater storage. Fig. 3 shows the relative proportions of the components of the optimal strength mixtures used in the experimental work.

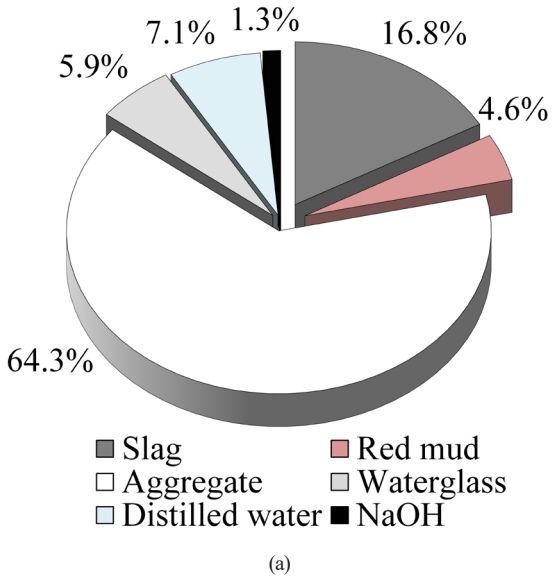

(a)

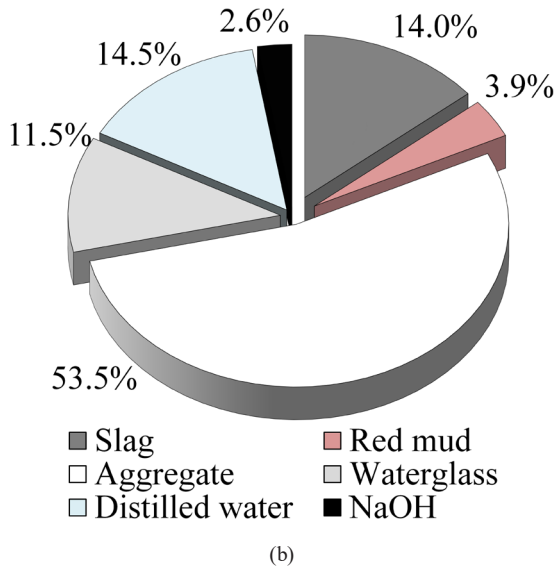

(b)

Fig. 3 Compositions of AAC mortars obtained by using the optimal: (a) red mud content and (b) L/S ratio

2.3 Methods

Qualitative and quantitative phase analyses of GGBFS, RM, and GW were performed using a Philips PW 3710 X-ray diffractometer with CuKα (50 kV, 40 mA) radiation. The velocity was set to 0.02° 2θ/s (in the 2θ range of 10–70°), and the instrument was equipped with a graphite monochromator. The instrument was controlled, and the data were collected, using X'Pert Data Collector software [43]. To determine the quantities of crystalline phases and the amorphous fraction, the internal standard method (Rietveld refinement) was applied. The X'Pert HighScore Plus software and the ICDD PDF-2 reference database were used to evaluate the X-ray diffractograms and perform Rietveld analysis.

The chemical compositions of the GGBFS, RM, and GW were determined using a Philips Axios PW 4400/24 wavelength-dispersive X-ray fluorescence analyzer. Melt sample preparation was used, with a sample-to-solvent mass ratio of 1.8 and a solvent of $Li_2B_4O_7$ + $LiBO_2$. The analysis was performed according to EN 196-2:2013 [44].

The particle size distribution and median (D50) of GGBFS, RM, and GW (sieved 63-0 μm and high-energy ground powders, respectively) were determined using a Fritsch Laser Particle Sizer Analysette 22 Next Nano type laser granulometer (laser wavelength: 532 nm, measuring range: 0.01-3,800 μm; measuring principle: Fraunhofer deflection). Before beginning the tests, the equipment dispersed and eliminated intergranular aggregation of the samples in a water bath with an ultrasonic mixer and pump for 30 seconds.

High-energy grinding of soda-lime glass waste was carried out using a Fritsch Pulverisette 5/2 planetary mill fitted with two 500 cm^3 stainless steel jars and 10 mm steel grinding balls. The mass ratio of the sample to the grinding balls was fixed at 1:11 during grinding.

The strength properties of the produced AAC samples were characterized by their compressive strength. CONTROLS Automax5 equipment was used to perform the measurements. Before starting the test, the surfaces of all specimens were ground flat and parallel. The tests were carried out in accordance with the relevant cement standard – EN 196-1 [41] – using a load force of 2400 N/s; however, the specimen size differed from the standard (ø 30 × 30 mm cylinders were tested). Due to the large number of varied experimental parameters in the present study, strength tests were only performed on most of the AAC specimens at 7 days of age. These parameters included the variable red mud content, the particle size

fractions of the glass waste (combined with different liquid-to-solid ratios), and the grinding intensity of the glass waste. However, tests were also performed after 28 days for the mixtures with the optimum compositions.

The morphology of the glass powders obtained through high-energy grinding, as well as that of the AACs produced, was investigated using an FEI/ThermoFisher Apreo S scanning electron microscope – operating in low vacuum mode – and a computer-controlled imaging system. The accelerating voltage was set to 5 kV for backscattered electron imaging and 10 kV for secondary electron imaging.

IR spectra of AAC mortars stored in air and underwater were obtained using a PerkinElmer Spectrum Two type FT-IR spectrometer in ATR (diamond crystal) mode.

Powder leaching tests were performed on GGBFS, RM, and CEM I powders, as well as on test specimens prepared from mixtures of optimum compositions (AAC and traditional binder), according to the TCLP (Toxicity Characteristic Leaching Procedure) standard [45]. The procedure involved the following steps. 50 g of solids were added to 1 l of leaching solution. The mixture was then left to stand at room temperature for 18 hours, with constant stirring at 100 rpm. After 90 minutes, the mixture was left to settle, then filtered, and the pH adjusted (1.3 ± 0.1) and stored in a refrigerator. The criterion for the test is a particle size of less than 1 cm, which was achieved for mortars using a Fritsch Disk Mill PULVERISETTE 13 Classic Line. The pH of the solutions was measured using an Orion 420A pH meter and electrode. The leach solutions were mixed using an IKA RCT Basic heated magnetic stirrer.

The monolithic (block) phase leaching test of AAC and CEM I mortars of optimum compositions was carried out in accordance with ANSI/ANS 16.1-2019 [46]. The cylindrical specimens were placed in a plastic dish containing 0.5 liters of distilled water and secured to the dish's airtight lid with thread and adhesive tape. Experiments began the day after mixing (i.e., on day 2), with the leaching medium being replaced on day 7. The complete test was then carried out until the samples were 28 days old.

The adsorption capacity of AAC- and CEM I-based mortars with optimal compositions was determined using 2 g of powdered material (with a particle size of <1 mm, powdered using a Fritsch Disk Mill PULVERISETTE 13 Classic Line) and a solution with a Pb^{2+} concentration of 50 ppm and a volume of 250 ml. The pH of the solution was adjusted to 4 using concentrated nitric acid (to reduce hydrolysis). The solid was stirred in the solution for 5 minutes, after which samples were taken at 5, 10, and 15 minutes. These experimental parameters were chosen based on the work of Chen et al. [27]. Adsorption studies were performed at 7 and 28 days of age of the test samples.

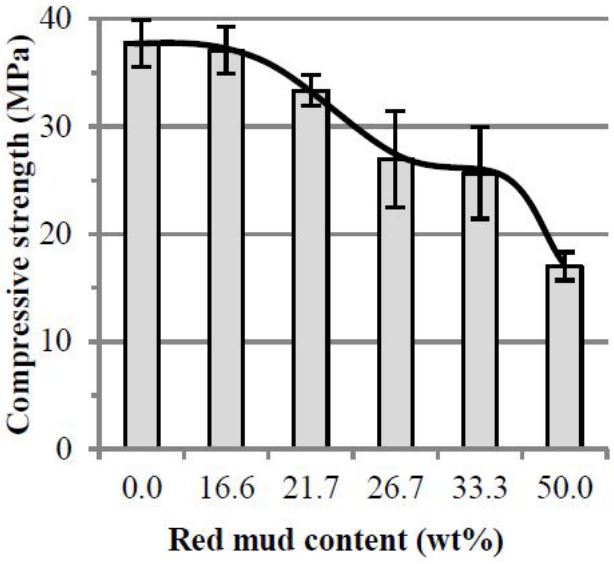

Fig. 4 The compressive strength of AAC specimens with different red mud content at 7 days of age

The heavy metal ion content of the homogenized leach solutions and the samples obtained from the adsorption experiments was determined using a SPECTRO FLAME MODULA E (Spectro GmbH) ICP-OES instrument with a horizontal-position axial plasma torch. Argon gas with a purity of 4.6 (99.996 %) was used as the plasma gas, meeting the requirements for spectroscopic-grade gases.

3 Results and discussion

3.1 Experiments to determine the optimal RM content

In the first stage of the experiments, blast furnace slag-based AAC mortars were prepared without red mud and used as controls. Then, GGBFS was partially replaced with red mud until the amounts of GGBFS and red mud (RM) were equal. Fig. 4 shows the compressive strength values of the AAC mortars with different red mud contents.

The compressive strength of the control samples (without red mud) is 37.7 MPa and can be maintained with a red mud content of 16.6 wt%. However, further increasing the RM content leads to a significant decrease in strength. In Fig. 4, two steeper parts are observed: one after an RM content of 21.7 wt% and the other after an RM content of 33.3 wt%. Up to the first breakpoint, a 12% decrease in strength is observed, followed by a more drastic decrease of ~30% in the middle stage (RM content = 26.7–33.3 wt%). Finally, at an RM content of 50.0 wt%, only about half of the initial value (17.0 MPa) is measured. This strength loss is

attributed to the reduced reactivity and limited gel-forming capacity of red mud, which is more crystalline and less reactive than GGBFS. At high replacement levels, the reactive slag content becomes insufficient to form a continuous binding matrix. Furthermore, RM has a significant iron content, and the Fe^{3+} ions in hematite slow down bonding, inhibiting gel formation and resulting in a weaker structure. Bayat et al. [32] obtained similar results when increasing the red mud content of AAC mortars at the expense of slag. After seven days, an RM content of 10 wt% does not significantly change the strength values. An RM content of 20 wt% results in a slight decrease. However, at higher amounts (40 wt%), a more significant difference is observed.

Even if the AAC matrix is capable of binding large amounts of red mud and thus significantly reducing the amount of waste, it is important to note that the aim of the present research is to ensure that the red mud content does not cause a drastic deterioration in the compressive strength. To achieve this, the use of red mud content at 21.7 wt% (GGBFS+RM by weight) is recommended. With this content, the corresponding samples have a compressive strength of 33.4 MPa, which exceeds the minimum strength class (32.5 MPa) required by the product standard for classical binders (EN 197-1). This statement is intended only as a point of reference, not as a formal claim of conformity.

Considering all the binder's components, the red mud content is 4.6 wt% (see Fig. 3(a)) in the AAC mortar. With the addition of 16.8 wt% blast furnace slag, the total waste material content is 21.4 wt%. In the spirit of the green economy and zero-waste approaches, the goal was to increase the amount of waste bound in the matrix by replacing standard quartz sand with an alternative aggregate, fractionated glass waste.

3.2 Experiments with fractionated glass waste

The next step in the experiment was to replace the standard sand with soda-lime glass waste. While a liquid-to-solid ratio of 0.15 was sufficient for the workability of the sand-containing samples, it proved insufficient when using fine-grained fractionated glass waste. Different L/S ratio mixtures were prepared to ensure the paste had the proper consistency. The L/S ratio choice was based on the consistency of the mixtures (Fig. 5).

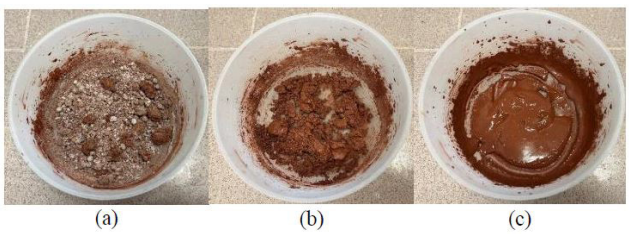

Fig. 5 Consistency of mixtures prepared using different L/S ratios ((a) little, (b) optimal amount, and (c) a lot of activating solution)

If the amount of activating solution was insufficient, the mixture would become lumpy (Fig. 5(a)). If too much solution was added, the mixture would become runny (Fig. 5(c)). In both cases, the mixture was difficult to handle, which resulted in lower strength values. The goal for all fractions was to achieve the so-called "earthy wet" consistency (Fig. 5(b)), which has sufficient moisture content for workability. It is slightly "runny" and less spreadable. Thus, it presumably provides the most compact and solid structure. For each GW fraction, the optimum consistency between the two endpoints was sought, requiring the addition of intermediate points. The compressive strength values obtained using different L/S ratios are given in Table 4.

Table 4 Effect of different particle size fractions of GW and varying L/S ratios on the compressive strength of AAC mortars at 7 days of age

L/S ratio	Compressive strength for different particle size fractions of GW (MPa)			
	1000-500 µm	500-250 µm	250-63 µm	63-0 µm
0.150	12.1 ± 1.5	12.1 ± 1.5	1.4 ± 0.6	-
0.188	20.4 ± 1.3*	-	-	-
0.225	12.9 ± 4.6	16.8 ± 1.4*	-	-
0.263	6.2 ± 2.1	12.1 ± 2.3	-	-
0.300	-	11.7 ± 0.1	14.9 ± 0.4*	20.0 ± 1.4
0.350	-	-	12.5 ± 0.8	25.3 ± 1.3*
0.375			10.5 ± 2.1	21.8 ± 1.00

* mixture with the best consistency

For each fraction, there is a correlation between the experiences obtained during mixing and the compressive strength values at 7 days of age. In all cases, the mixture marked "best consistency" (*) gave the maximum strength. This consistency was selected based on visual assessment and practical workability during mixing, corresponding to the so-called "earthy wet" state illustrated in Fig. 5(b). Although no instrumental measurement was applied, this consistency consistently resulted in the highest compressive strength values, thus confirming its suitability as the optimal mixture condition. As shown in Table 4, reducing the particle size of fractionated glass waste up to a fraction above 63 µm leads to a decrease in strength values. In contrast, a fraction below 63 µm increases the strength due to the filler effect and the pozzolanic activity of the fine particles. Nevertheless, the optimal value of 25.3 MPa is approximately 25% lower than that of the standard quartz

sand mixture (33.4 MPa). This is because the GW particle size distribution is insufficiently wide: it lacks the larger particles that would directly increase the mechanical strength. In standard sand, however, it is the combination of the large particles and fine fractions that has a positive effect on the strength of the material. A similar phenomenon was observed by Zhang et al. [39], who studied the effect of GW particle size on the strength. Their experiments demonstrated that if the GW particle size (D50) exceeds 300 µm, the material does not exhibit chemical reactivity. However, when the D50 value is smaller than 45 µm, the GW can react with the activating solution, incorporating into the gel structure and improving the mechanical properties. The D50 value of the 63-0 µm fraction we used is 38.7 µm, meaning it can participate as a pozzolanic component in the alkali activation process. In the following, our goal was to increase the reactivity of GW with the help of high-energy grinding.

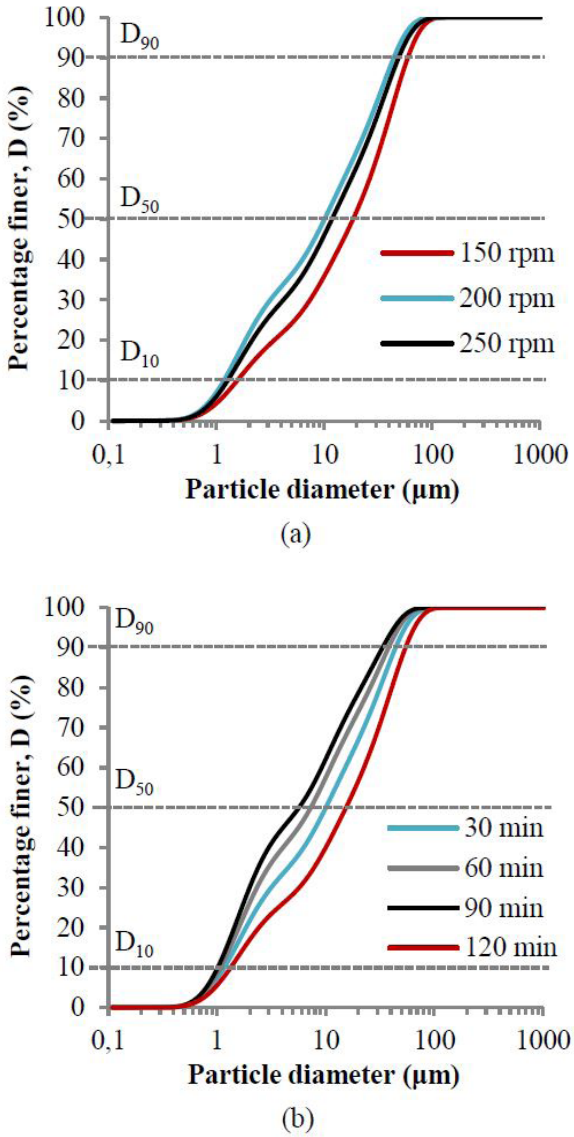

Fig. 6 Particle size distribution curves of GW grindings obtained using different (a) rotation speed and (b) grinding time

3.3 Effect of high-energy grinding of GW on strength

Based on the results and experience of the second series of experiments, it is expected that the glass waste particles, if sufficiently fine, will react with the activating solution. To prove this theory and to increase the strength values, the GW was subjected to high-energy grinding. In the process, a GW fraction between 500 and 250 µm was used (this fraction was the largest in the original glass waste). First, the rotation speed was varied (150, 200, and 250 rpm) using a constant grinding time of 30 minutes. Then, considering the compressive strength values, the grinding time was modified (30, 60, 90, and 120 minutes) at a constant speed (200 rpm). Preliminary observations showed that the resulting grindings were most similar in fineness to the fraction below 63 µm, as confirmed by the particle size distribution curves presented later (Fig. 6). For this reason, all grindings were mixed using an L/S ratio of 0.350, as this ratio gave the highest strength for the fraction below 63 µm.

The analysis of the particle size of the grindings showed that increasing both the rotation speed and the grinding time caused a decrease in the primary particle size. However, beyond certain thresholds (200 rpm for speed and 90 minutes for grinding time), the amount of secondary particles increases. Thus, aggregates/agglomerates formed, and the particle size coarsened (see Fig. 7).

Based on the results in Fig. 6, the compressive strength values should theoretically form a maximum curve. The maximum value is associated with the best ratio of fine primary particles to few secondary particles, as this combination has the strongest potential reactivity. According to the obtained values, the optimum is expected at a rotation speed of 200 rpm and a grinding time of 90 minutes. Fig. 8 summarizes the compressive strength results for the specimens produced from the grindings.

For materials of similar hardness, the optimum rotation speed is around 200 rpm. Based on the results in Fig. 8(a), this rotation speed was exactly 200 rpm for GW, at which point the strength reached its maximum value of 42.0 MPa. At lower speeds, the particle size is insufficient to increase the pozzolanic activity. At higher speeds, the particle size would be sufficient; however, the primary particles may stick together, creating secondary particles (the aggregation/agglomeration effect). This is confirmed by the particle size distribution curves and SEM images of the

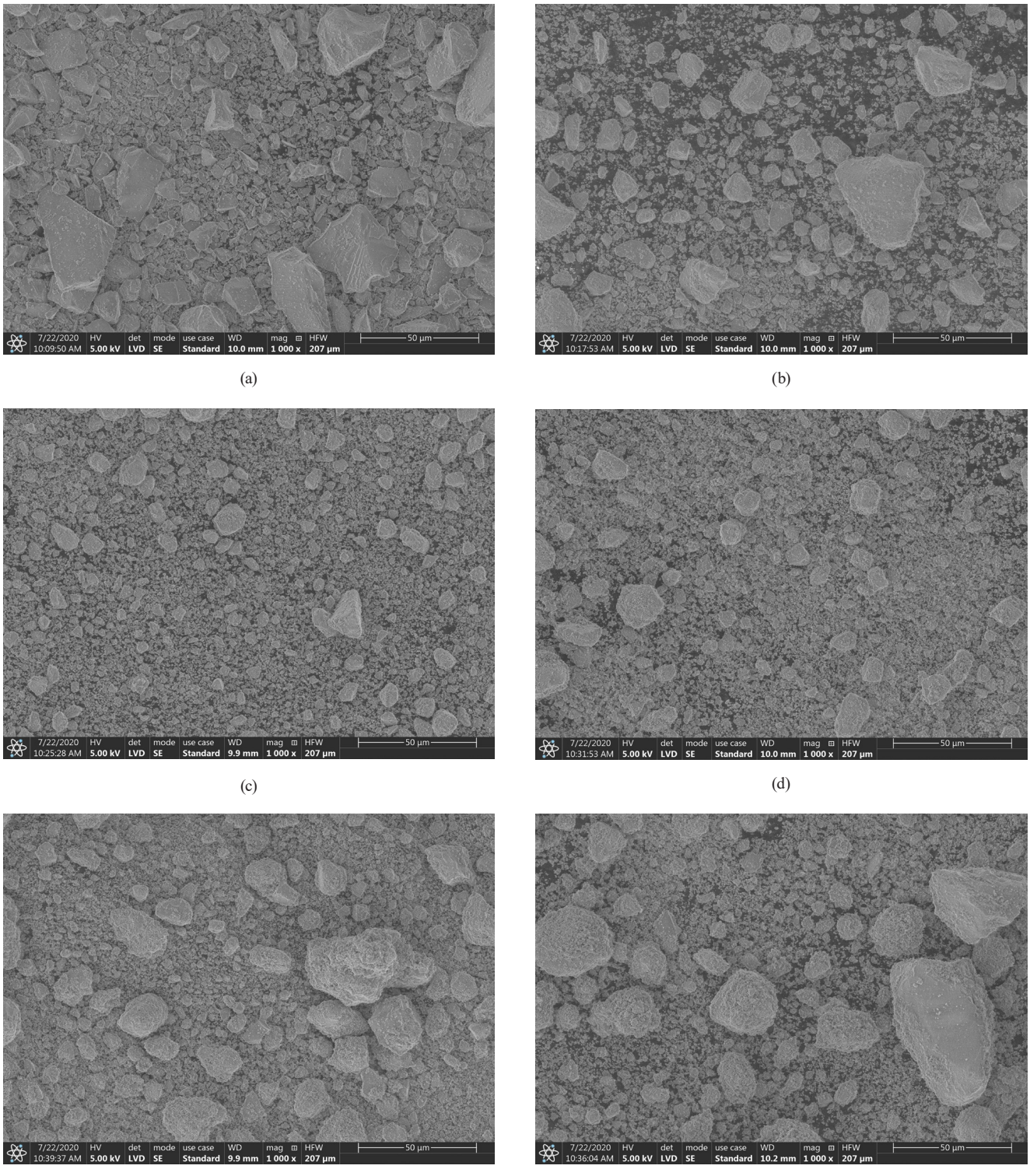

Fig. 7 Effect of grinding parameters on glass powder morphology: (a) 30 min – 150 rpm, (b) 30 min – 200 rpm, (c) 30 min – 250 rpm, (d) 60 min – 200 rpm, (e) 90 min – 200 rpm, and (f) 120 min – 200 rpm

grindings (Figs. 6(a) and 7(a)–(c)). The maximum strength value achieved is 2.5 times higher than the relevant value for the unground 500–250 µm fraction (16.8 MPa) and approximately 1.7 times higher than the relevant value for the 63–0 µm fraction (25.3 MPa).

Fig. 8(b) shows that increasing the grinding time has a positive effect on the strength values up to a certain point. Up to a grinding time of 90 minutes, the strength values increase monotonically. However, a further increase in the grinding time has a negative effect on the results. This

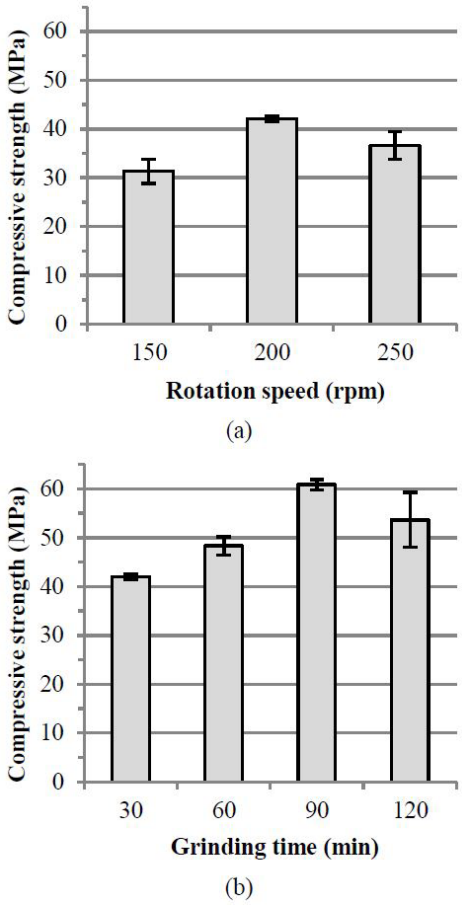

Fig. 8 Effect of high-energy grinding of GW on the compressive strength at 7 days using different (a) rotation speeds and (b) grinding times

decrease is attributed to the agglomeration of fine particles caused by excessive mechanical energy input during prolonged grinding (see Figs. 7(b) and 7(d)–(f)), which reduces the effective reactivity and compromises the compactness of the hardened structure. The maximum strength value achieved (60.9 MPa) is 3.6 times higher than the relevant value for the unground 500-250 μm fraction (16.8 MPa) and 2.4 times higher than the relevant value for the 63-0 μm fraction (25.3 MPa). It is important to note that the compressive strength values of the developed AAC mortars (53.7 and 60.9 MPa) exceed the value of the third strength class (42.5 MPa) specified in the product standard (EN 197-1). Though the test specimens were not the standard size required for cement mortar tests, these results are significant and encouraging for developing alternative binders.

3.4 Comparative tests of AAC and CEM I mortars

In the final stage of the experiments, the physical properties of the AAC system (containing GGBFS, RM, and high-energy ground GW) were compared with the relevant values of CEM I-based mortars. There are no existing standard specifications for the storage of AACs, but there are strict instructions (EN 12390-2 [45]) for traditional binders. Since one of the comparative studies, the monolithic (block) phase leaching method, is very similar to the underwater storage of traditional binders, it was considered important to investigate the effect of changing the storage method on the strength values for the developed AAC composite. The standard quartz sand-containing AAC system was also included in the experiments to obtain a more complete overview (this system was also tested in the leaching and adsorption experiments). For the CEM I system, the effect of air storage was not tested, as it is not the standard for determining the standard properties (e.g., compressive strength). The relevant measurements were carried out at both 7 and 28 days of age, and the results are summarized in Fig. 9. In the diagram, G indicates AAC mortar with glass waste, S indicates AAC mortar with sand, and CEM I indicates mortar with normal Portland cement.

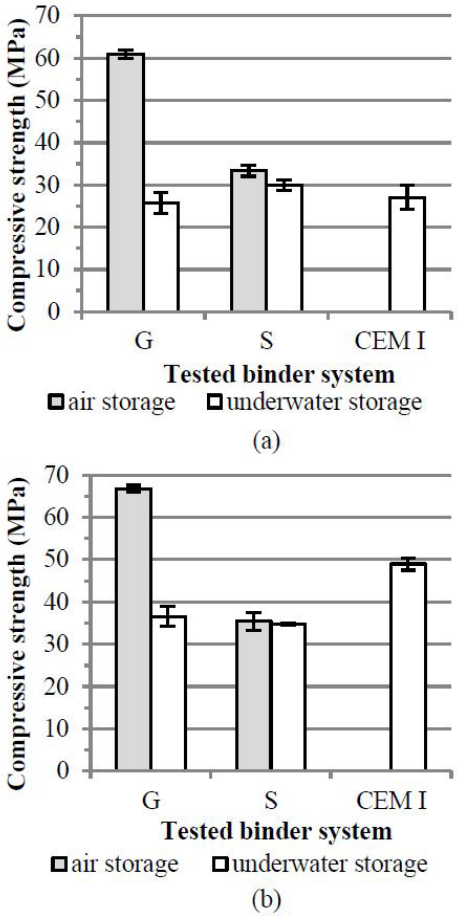

Fig. 9 Effect of storage conditions on strength at (a) 7 and (b) 28 days of age (G: AAC with glass waste, S: sand-containing AAC, CEM I: Portland cement-based mortar)

Fig. 9 shows that using the underwater storage method instead of the air storage method for the sand-containing AAC mortar did not significantly affect the compressive strength values (a 10% decrease at 7 days and only a 2% decrease at 28 days). This minor decrease is likely due to physical curing effects, as the inert quartz sand does not participate in the geopolymerization process, and no substantial change in hydration products is expected. Moreover, the observed strength differences are within the experimental standard deviation. However, the glass-containing system behaved very differently. A drastic decrease in strength was observed at 7 and 28 days, with reductions of 60% and 45%, respectively. On the other hand, after 28 days, the product stored in air (A) exceeded the maximum strength class (52.5 MPa), as required by EN 197-1 (GA: 66.8 MPa). For underwater storage (Uw), the products only met the minimum strength class requirement of 32.5 MPa (G-Uw: 36.5 MPa and S-Uw: 34.8 MPa). The strength values of the CEM I system were as expected.

The difference in strength values between AAC composites containing glass waste stored in air and underwater is due to the formation of different quality hydration products. Fig. 10 shows the results of FT-IR studies performed to interpret these changes.

As shown in Fig. 10, the vibrations are consistent for both the air- and underwater-stored samples. However, the transmittance values vary, and the spectra exhibit a distinct fine structure. The most significant difference is observed in the "fingerprint" band characteristic of AACs. Underwater storage weakens the band between 950 and 1000 cm^{-1} and shifts it towards higher wavenumbers. This phenomenon may be indicative of a partial transformation of the Si–O–Si and Al–Si–O bonds (e.g., due to rearrangement or dissolution). Another change observed

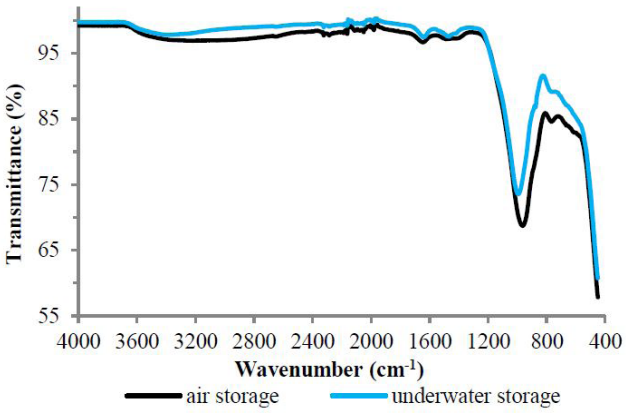

Fig. 10 FT-IR spectra of AAC samples stored in different conditions

was a decrease in transmittance in the 400–800 cm^{-1} band (bending vibrations of Si–O–Si and Al–Si–O bonds), suggesting that the system contains fewer bound phases. The slight increase in the bands characteristic of −OH groups (~3400 cm^{-1} and ~1640 cm^{-1}) indicates the presence of more bound/adsorbed water.

Underwater storage can lead to the leaching of Na^+ ions, resulting in a weaker gel structure. This phenomenon was observed by Dong et al. [15], who investigated the effect of storage conditions on the strength of AACs based on fly ash and blast furnace slag. They found that Na^+ and OH^- ions can be released from the pore solution by diffusion. As alkalinity decreases, polycondensation slows down or reverses, resulting in a lower degree of cross-linking. In our case, the high glass powder content (53.5 wt%) may further worsen the situation. Without the alkaline medium necessary for dissolution and polycondensation of the high amorphous content, gel formation may stop. In this case a part of the glass powder remains in its original, unreacted state. To further support this explanation, SEM imaging was performed on the fractured surfaces of the hardened AAC specimens (see Fig. 11).

The micrographs revealed the presence of angular, smooth-surfaced particles embedded in the matrix, which can be attributed to unreacted glass powder. These features are especially pronounced in the underwater-cured samples, indicating insufficient dissolution and gel formation due to reduced alkalinity. No significant reaction rims or interface densification were observed around the particles, further confirming their largely inert behavior under these conditions. Consequently, a stable, well-cross-linked gel did not form; instead, a weak, disordered matrix formed, resulting in a deterioration in strength values.

The leaching of the alkali content indicates that other elements, including heavy metals, may also be released from the matrix. To establish this assumption, powder and monolithic (block) phase leaching studies were performed as described in Subsection 2.3, Methods. The results of the powder leaching tests on the raw materials (GGBFS, RM, and CEM I) and their test specimens (AACs containing red mud, sand (S), or high-energy ground glass waste (G), and CEM I-based mortar) are summarized in Table 5. The table contains the health limit concentrations for the analyzed heavy metals in drinking water (according to Governmental Decree No. 201/2001 (X. 25.) on "Quality Requirements for Drinking Water and the Monitoring Procedure" [47]). It also includes the lower measurement limits of the ICP device and the measurement error values.

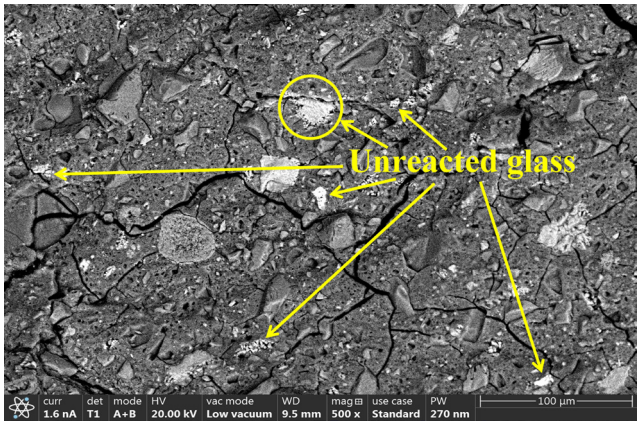

(a)

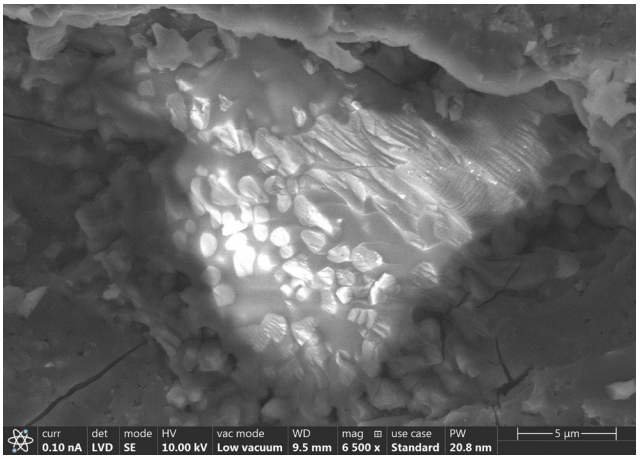

(b)

Fig. 11 SEM images of AAC samples containing glass powder stored underwater (a) BSE imaging of the matrix and (b) SE imaging of the unreacted glass (the detail circled in the BSE image can be seen in larger magnification in the SE image)

Table 5 Results of powder leaching tests on raw materials and 28-day samples; health limits for drinking water; and ICP instrument lower limits and error values

Tested Material	Concentrations of tested heavy metals (µg/l)						
	Cu	Cr	Ni	Pb	Cd	Hg	Zn
GGBFS	n.m.	31	11	n.m.	4	29	26
RM	n.m.	n.m.	34	57	n.m.	532	56
S AAC	16	39	n.m.	111	n.m.	72	57
G AAC	n.m.	73	n.m.	133	n.m.	8	33
CEM I	104	637	24	104	n.m.	n.m.	51
CEM I mortar	n.m.	265	n.m.	67	n.m.	24	112
Health limit	2000	50	20	10	5	1	n.l.
Lower limit of measurement	15	19	6	39	4	7	5
Error (%)	2	1	0.5	5	0.1	1.5	0.1

n.l.: no limit values given according to Governmental Decree No. 201/2001 (X. 25.) on "Quality Requirements for Drinking Water and the Monitoring Procedure" [47]
n.m.: not measurable, below the lower limit of the ICP device

From the data in Table 5, it can be seen that no health concentration limit is specified for zinc; in this case, the aim was to achieve the lowest possible value. Measurements showed higher concentrations of Hg in blast furnace slag, Ni, Pb, and Hg in red mud, and Cr, Ni, and Pb in Portland cement than the allowed limit. The source of the metal content is iron ore in blast furnace slag, bauxite in red mud, and various contaminants in clay and limestone (in summary: raw materials) in Portland cement. AAC composites have a better immobilization capacity for Cr and Zn than CEM I-based mortars but perform worse for Pb. Ni and Cd concentrations were below the lower limit of measurement for all systems, and Cu, Pb, and Hg concentrations depended on the type of AAC. S AAC binds Cr and Pb better than its glass-based counterpart, but immobilization of Cu, Hg, and Zn is preferable with G AAC.

It is important to note that the amount of raw materials in the hardened samples was less than 50 g (this is the amount required to perform powder leaching tests). Therefore, the weights are not identical, and the heavy metal concentrations obtained and the conclusions drawn are only indicative. However, it has been demonstrated that the leaching of some heavy metals (Cr, Pb, Hg) is significant under acidic conditions when subjected to strong fragmentation. For this reason, it was considered appropriate to carry out more "realistic" monolithic (block) phase leaching tests, the results of which are summarized in Table 6.

As shown in Table 6, the leaching of the tested material systems is lower up to day 7 than in the following period. Although copper has the highest leaching rate, its concentration never reaches the health limit. However, this is not true for chromium, cadmium, and mercury, all of which have concentrations above the health limit. It should be highlighted that chromium does not leach from the sand-containing AAC in detectable quantities; therefore, the total metal concentration in this system is the lowest.

Although the total concentration of heavy metals leached from the AAC composite containing red mud and glass waste exceeds the relevant value for CEM I mortar, the immobilization capacity of Cu, Cd, and Hg is better than that of the classical binder. The most significant difference is due to Zn leaching; however, no concentration limit is specified for this heavy metal in the relevant government regulation. The performance of G AAC- and CEM I-based mortars is similar regarding the total heavy metal content released, with a difference of 8.7%. Sun et al. [28] made a similar finding when they compared the heavy metal leaching of RM-containing AACs with the relevant values of

Table 6 Results of monolithic (block) phase leaching tests on AAC and CEM I based mortars and health limits for drinking water

	Concentrations of tested heavy metals (µg/l)							
	Cu	Cr	Ni	Pb	Cd	Hg	Zn	Total
S AAC day 2-7	70	n.m.	n.m.	n.m.	n.m.	n.m.	29	99
S AAC day 7-28	51	n.m.	n.m.	n.m.	46	23	32	152
S AAC full period	121	n.m.	n.m.	n.m.	46	23	61	251
G AAC day 2-7	111	n.m.	n.m.	n.m.	10	20	93	234
G AAC day 7-28	172	247	n.m.	n.m.	26	57	103	605
G AAC full period	283	247	n.m.	n.m.	36	77	196	839
CEM I mortar day 2-7	390	n.m.	n.m.	n.m.	9	10	n.m.	409
CEM I mortar day 7-28	n.m.	201	n.m.	n.m.	35	112	15	363
CEM I mortar full period	390	201	n.m.	n.m.	44	122	15	772
Health limit	2000	50	20	10	5	1	n.l.	-

n.l.: no limit values given according to Governmental Decree No. 201/2001 (X. 25.) on "Quality Requirements for Drinking Water and the Monitoring Procedure" [47]
n.m.: not measurable, below the lower limit of the ICP device

classical binders. All the binder systems we investigated could bind the total lead content in the matrix. Therefore, we investigated whether AAC- and CEM I-based mortars could immobilize additional Pb^{2+} ions.

Red mud has an extremely high adsorption capacity for heavy metals due to its fine particle size and high specific surface area [19, 24]. According to some studies, red mud promotes the formation of phases in AACs suitable for adsorbing heavy metals from industrial wastewater [27]. To test this hypothesis, powder-based adsorption experiments were performed using Pb^{2+} ions. Measurements were taken at 7 and 28 days on binder systems (S AAC, G AAC, and CEM I-based mortars), which were used in previous comparative studies. The results are shown in Fig. 12. In the diagram, A indicates air storage, Uw indicates underwater storage, and 7n and 28n indicate 7 and 28 days, respectively. The adsorption capacity of the samples stored in air and underwater was tested for AAC composites, whereas only the adsorption capacity of the samples stored underwater was tested for CEM I-based mortars.

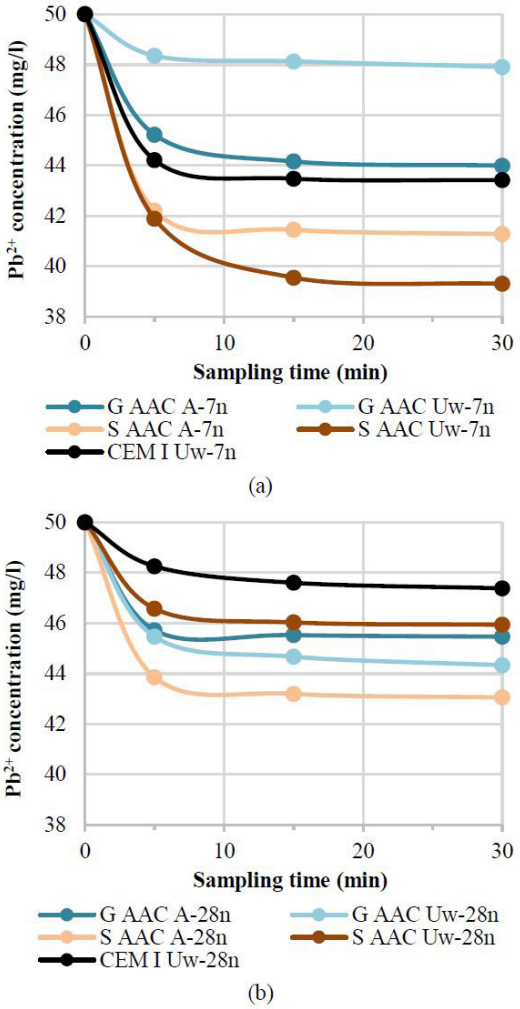

Fig. 12 The adsorption capacity of AAC and CEM I-based mortars at (a) 7 and (b) 28 days of age (A: air storage, Uw: underwater storage, 7n: 7-day, 28n: 28-day test specimen)

The results of the 7-day-old tests (Fig. 12(a)) show that some AACs perform better than CEM I mortar. This finding is promising for the use of alternative cement systems in this type of application. The adsorption capacity of the glass-based systems (blue curves in Fig. 12(a)) is weaker than that of CEM I-based mortar (black curve). When stored underwater, the binding rate is practically negligible. When stored in air, however, it approaches the relevant values for traditional binders. Using standard sand as a filler (brown curves) produced better results than CEM I for both storage methods. In this case, the specimens stored in water were able to bind more lead.

Examining the 28-day results (Fig. 12(b)) reveals that, in this case, all AACs outperformed the CEM I-based mortar. The adsorption rate is completely different from that observed after seven days, but it can be concluded

that almost all of the tested materials were able to absorb less lead after 28 days. The exception is the G AAC sample stored underwater, which had an increased adsorption capacity of 7.5% from 7 to 28 days. The Pb^{2+} adsorption capacity decreases in the following order: S AAC A > G AAC Uw > G AAC A > S AAC Uw > CEM I Uw.

For both adsorption measurements at 7 and 28 days of age, Pb^{2+} concentrations decreased significantly within the first 5 minutes, with a slight decrease at the second sampling point (15 minutes) and reaching equilibrium within 30 minutes. These results are consistent with those reported by Chen et al. [29]. Of the tested binder systems, S AAC Uw and S AAC A exhibited the greatest adsorption capacity at 7 and 28 days of age, with a 21.4% and 13.9% reduction in Pb^{2+} concentration. These results indicate that the adsorption capacity of the tested binders depends on the system type, additive type and quality, storage conditions, and test age.

4 Conclusions

This study investigated alkali-activated cement (AAC) composites incorporating industrial by-products – blast furnace slag (GGBFS), red mud (RM), and soda-lime glass waste (GW) – as potential sustainable alternatives for construction and environmental applications. Based on the experiments performed, the following conclusions can be drawn.

- The AACs can incorporate up to 50 wt% RM, but with a significant strength reduction. An optimal RM content of 21.7 wt% results in 33.4 MPa compressive strength, corresponding to the minimum strength class of traditional binders.
- GW can act both a reactive and inert component. Although glass-containing systems generally showed lower strength than sand-based ones, high-energy grinding (90 min, 200 rpm) increased reactivity, achieving up to 66.8 MPa – surpassing the value of EN 197-1 standard's maximum strength class (52.5 MPa).
- Underwater curing significantly reduced strength in GW-based AACs (up to 45%) due to Na^{+} and OH^{-} leaching, which hindered gel formation, as confirmed by FT-IR and SEM analyses.
- Powder-based heavy metal leaching tests showed AACs effectively immobilize Cd and Ni. While monolithic samples showed higher total heavy metal release than CEM I, their immobilization of Cu, Cd, and Hg was superior, and Pb retention was complete.
- Powder-based adsorption experiments confirmed that RM-containing AACs exhibit higher Pb^{2+} uptake than CEM I mortars, making them promising for wastewater treatment.

In addition to supporting the green economy and zero-waste approaches, AACs can bind large amounts of waste (71.4 wt% combined GGBFS, RM, and GW) and offer a way to safely recycle red mud without any pre-treatment. These products can serve as an alternative to widely used materials in the construction industry and in specific applications, such as heavy metal adsorbents.

Acknowledgement

Funded by the Research Fellowship Programme (Code: 2024-2.1.1-EKÖP) of Ministry of Culture and Innovation of Hungary from the National Fund for Research, Development and Innovation.

References

[1] Provis, J. L. "Alkali-activated materials", Cement and Concrete Research, 114, pp. 40–48, 2018. https://doi.org/10.1016/j.cemconres.2017.02.009

[2] Lanjewar, B. A., Chippagiri, R., Dakwale, V. A., Ralegaonkar, R. V. "Application of alkali-activated sustainable materials: a step towards net zero binder", Energies, 16(2), 969, 2023. https://doi.org/10.3390/en16020969

[3] Li, W., Tang, Z., Tam, V. W., Zhao, X., Wang, K. "A review on durability of alkali-activated system from sustainable construction materials to infrastructures", ES Materials & Manufacturing, 4(2), pp. 2–19, 2019. https://doi.org/10.30919/esmm5f204

[4] Kryvenko, P., Rudenko, I., Sikora, P., Sanytsky, M., Konstantynovskyi, O., Kropyvnytska, T. "Alkali-activated cements as sustainable materials for repairing building construction: a review", Journal of Building Engineering, 90, 109399, 2024. https://doi.org/10.1016/j.jobe.2024.109399

[5] Liang, Q., Huang, X., Zhang, L., Yang, H. "A Review on Research Progress of Corrosion Resistance of Alkali-Activated Slag Cement Concrete", Materials, 17(20), 5065, 2024. https://doi.org/10.3390/ma17205065

[6] Wu, T., Tang, S., Dong, Y. R., Luo, J. H. "A Review of the Thermal and Mechanical Characteristics of Alkali-Activated Composites at Elevated Temperatures", Buildings, 15(5), 738, 2025. https://doi.org/10.3390/buildings15050738

[7] Keane, P., Jacob, R., Trout, N., Clarke, S., Bruno, F. "Thermal stability of a waste-based alkali-activated material for thermal energy storage", Chemical Thermodynamics and Thermal Analysis, 3–4, 100014, 2021. https://doi.org/10.1016/j.ctta.2021.100014

[8] Palomo, A., Maltseva, O., Garcia-Lodeiro, I., Fernández-Jiménez, A. "Portland versus alkaline cement: continuity or clean break: a key decision for global sustainability", Frontiers in Chemistry, 9, 705475, 2021. https://doi.org/10.3389/fchem.2021.705475

[9] Nasir, M., Mahmood, A. H., Bahraq, A. A. "History, recent progress, and future challenges of alkali-activated binders–An overview", Construction and Building Materials, 426, 136141, 2024. https://doi.org/10.1016/j.conbuildmat.2024.136141

[10] Niş, A., Altındal, İ. "Compressive strength performance of alkali activated concretes under different curing conditions", Periodica Polytechnica Civil Engineering, 65(2), pp. 556–565, 2021. https://doi.org/10.3311/PPci.17016

[11] Kumar, A., Saravanan, T. J., Bisht, K., Kabeer, K. S. A. "A review on the utilization of red mud for the production of geopolymer and alkali activated concrete", Construction and Building Materials, 302, 124170, 2021. https://doi.org/10.1016/j.conbuildmat.2021.124170

[12] Khairul, M. A., Zanganeh, J., Moghtaderi, B. "The composition, recycling and utilisation of Bayer red mud", Resources, Conservation and Recycling, 141, pp. 483–498, 2019. https://doi.org/10.1016/j.resconrec.2018.11.006

[13] Bayat, A., Hassani, A., Azami, O. "Thermo-mechanical properties of alkali-activated slag–Red mud concrete", Road Materials and Pavement Design, 21(2), pp. 411–433, 2020. https://doi.org/10.1080/14680629.2018.1500299

[14] de Gutiérrez, R. M., Villaquirán-Caicedo, M. A., Guzmán-Aponte, L. A. "Alkali-activated metakaolin mortars using glass waste as fine aggregate: Mechanical and photocatalytic properties", Construction and Building Materials, 235, 117510, 2020. https://doi.org/10.1016/j.conbuildmat.2019.117510

[15] Dong, M., Elchalakani, M., Karrech, A. "Curing conditions of alkali-activated fly ash and slag mortar", Journal of Materials in Civil Engineering, 32(6), 04020122, 2020. https://doi.org/10.1061/(ASCE)MT.1943-5533.0003233

[16] Akyüncü, V., Avşar, Y. E., Emre, T. E. "Effect of Activator Type on Geopolymer Mortars Containing Different Types of Fly Ash", Periodica Polytechnica Civil Engineering, 67(3), pp. 757–764, 2023. https://doi.org/10.3311/PPci.21945

[17] Sutar, H., Mishra, S. C., Sahoo, S. K., Maharana, H. S. "Progress of red mud utilization: An overview", American Chemical Science Journal, 4(3), pp. 255–279, 2014. https://doi.org/10.9734/ACSJ/2014/7258

[18] Archambo, M., Kawatra, S. K. "Red mud: fundamentals and new avenues for utilization", Mineral Processing and Extractive Metallurgy Review, 42(7), pp. 427–450, 2021. https://doi.org/10.1080/08827508.2020.1781109

[19] Wang, J., Liu, X., Zhang, Z., Liu, Y. "Synergistic utilization, critical mechanisms, and environmental suitability of bauxite residue (red mud) based multi-solid wastes cementitious materials and special concrete", Journal of Environmental Management, 361, 121255, 2024. https://doi.org/10.1016/j.jenvman.2024.121255

[20] Winkler, D., Bidlo, A., Bolodár-Varga, B., Erdő, Á., Horváth, A. "Long-term ecological effects of the red mud disaster in Hungary: Regeneration of red mud flooded areas in a contaminated industrial region", Science of The Total Environment, 644, pp. 1292–1303, 2018. https://doi.org/10.1016/j.scitotenv.2018.07.059

[21] Gelencsér, A., Kováts, N., Turóczi, B., Rostási, Á., Hoffer, A., Imre, K., ..., Pósfai, M. "The red mud accident in Ajka (Hungary): characterization and potential health effects of fugitive dust", Environmental Science & Technology, 45(4), pp. 1608–1615, 2011. https://doi.org/10.1021/es104005r

[22] Wang, L., Sun, N., Tang, H., Sun, W. "A review on comprehensive utilization of red mud and prospect analysis", Minerals, 9(6), 362, 2019. https://doi.org/10.3390/min9060362

[23] Alam, S., Das, S. K. "Characterization of Phosphogypsum Blended Red Mud as Geo-material", Periodica Polytechnica Civil Engineering, 69(1), pp. 231–238, 2025. https://doi.org/10.3311/PPci.37270

[24] Wang, M., Liu, X. "Applications of red mud as an environmental remediation material: A review", Journal of Hazardous Materials, 408, 124420, 2021. https://doi.org/10.1016/j.jhazmat.2020.124420

[25] Arroyo, F., Luna-Galiano, Y., Leiva, C., Vilches, L. F., Fernández-Pereira, C. "Environmental risks and mechanical evaluation of recycling red mud in bricks", Environmental Research, 186, 109537, 2020. https://doi.org/10.1016/j.envres.2020.109537

[26] Lyu, F., Hu, Y., Wang, L., Sun, W. "Dealkalization processes of bauxite residue: a comprehensive review", Journal of Hazardous Materials, 403, 123671, 2021. https://doi.org/10.1016/j.jhazmat.2020.123671

[27] Chen, X., Guo, Y., Ding, S., Zhang, H., Xia, F., Wang, J., Zhou, M. "Utilization of red mud in geopolymer-based pervious concrete with function of adsorption of heavy metal ions", Journal of Cleaner Production, 207, pp. 789–800, 2019. https://doi.org/10.1016/j.jclepro.2018.09.263

[28] Sun, Z., Tang, Q., Xakalashe, B. S., Fan, X., Gan, M., Chen, X., ..., Friedrich, B. "Mechanical and environmental characteristics of red mud geopolymers", Construction and Building Materials, 321, 125564, 2022. https://doi.org/10.1016/j.conbuildmat.2021.125564

[29] Awad, A., Akcaoglu, T., Cubukcuoglu, B., Canpolat, O. "Experimental investigation of mechanical properties of geopolymer mortars produced with metakaolin, red mud and glass powder", Computers and Concrete, 27(6), pp. 597–606, 2021. https://doi.org/10.12989/cac.2021.27.6.597

[30] Occhicone, A., Vukčević, M., Bosković, I., Ferone, C. "Red mud-blast furnace slag-based alkali-activated materials", Sustainability, 13(20), 11298, 2021. https://doi.org/10.3390/su132011298

[31] Zhang, M., Zhao, M., Zhang, G., Mann, D., Lumsden, K., Tao, M. "Durability of red mud-fly ash based geopolymer and leaching behavior of heavy metals in sulfuric acid solutions and deionized water", Construction and Building Materials, 124, pp. 373–382, 2016. https://doi.org/10.1016/j.conbuildmat.2016.07.108

[32] Bayat, A., Hassani, A., Yousefi, A. A. "Effects of red mud on the properties of fresh and hardened alkali-activated slag paste and mortar", Construction and Building Materials, 167, pp. 775–790, 2018. https://doi.org/10.1016/j.conbuildmat.2018.02.105

[33] Erol, F., Al-mashhadani, M. M., Aygörmez, Y., Niş, A. "Effect of ceramic waste powder content and sodium hydroxide molarity on the residual mechanical strength of alkali-activated mortars", Materials Chemistry and Physics, 309, 128403, 2023. https://doi.org/10.1016/j.matchemphys.2023.128403

[34] Alam, S., Das, S. K., Rao, B. H. "Strength and durability characteristic of alkali activated GGBS stabilized red mud as geo-material", Construction and Building materials, 211, pp. 932–942, 2019. https://doi.org/10.1016/j.conbuildmat.2019.03.261

[35] Peduzzi, P. "Sand, rarer than one thinks", Environmental Development, 11(208–218), 682, 2014. https://doi.org/10.1016/j.envdev.2014.04.001

[36] Rangel-Buitrago, N., Neal, W., Pilkey, O., Longo, N. "The global impact of sand mining on beaches and dunes", Ocean & Coastal Management, 235, 106492, 2023. https://doi.org/10.1016/j.ocecoaman.2023.106492

[37] Uysal, M., Dilbas, H., Çoşgun, T., Bendjilali, F. "Red-mud additive geopolymer composites with eco-friendly aggregates", Construction and Building Materials, 425, 135915, 2024. https://doi.org/10.1016/j.conbuildmat.2024.135915

[38] Jalalinejad, M., Hemmati, A., Mortezaei, A. "Mechanical and durability properties of sustainable self-compacting concrete with waste glass powder and silica fume", Periodica Polytechnica Civil Engineering, 67(3), pp. 785–794, 2023. https://doi.org/10.3311/PPci.21537

[39] Zhang, Y., Xiao, R., Jiang, X., Li, W., Zhu, X., Huang, B. "Effect of particle size and curing temperature on mechanical and microstructural properties of waste glass-slag-based and waste glass-fly ash-based geopolymers", Journal of Cleaner Production, 273, 122970, 2020. https://doi.org/10.1016/j.jclepro.2020.122970

[40] Adesina, A. "Durability and microstructural characteristics of alkali activated materials made with waste glass as precursor: A review", Cleaner Materials, 6, 100134, 2022. https://doi.org/10.1016/j.clema.2022.100134

[41] CEN "EN 1961 Methods of testing cement – Part 1: Determination of strength", European Committee for Standardization, Brussels, Belgium, 2016. https://doi.org/10.31030/2482416

[42] CEN "EN 123902 Testing hardened concrete – Part 2: Making and curing specimens for strength tests", European Committee for Standardization, Brussels, Belgium, 2019. https://doi.org/10.31030/3045734

[43] Malvern Panalytical B. V. "HighScore Plus (Version 5.0) [Computer software]", Almelo, the Netherlands, 2021.

[44] CEN "EN 1962 Methods of testing cement – Part 2: Chemical analysis of cement", European Committee for Standardization, Brussels, Belgium, 2013. https://doi.org/10.31030/2036285

[45] U.S. Environmental Protection Agency "EPA SW846 Method 1311: Toxicity Characteristic Leaching Procedure", U.S. Environmental Protection Agency, Washington, DC, USA, 1992. [online] Available at: https://www.Epa.Gov/Hw-Sw846/Sw-846-Test-Method-1311-Toxicity-Characteristic-Leaching-Procedure [Accessed: 05 May 2025]

[46] ANS "ANSI/ANS 16.12019 Measurement of the Leachability of Solidified Low-Level Radioactive Wastes by a Short-Term Test Procedure", American Nuclear Society, La Grange Park, IL, USA, 2019. [online] Available at: https://webstore.ansi.org/standards/ansi/ansians162019 [Accessed: 10 June 2025]

[47] Government of Hungary "201/2001. (X. 25.) Korm. rendelet az ivóvíz minőségi követelményeiről és az ellenőrzés rendjéről", (Governmental Decree No. 201 of 2001 (X. 25.) On Quality Standards for Potable Water and on Rules of Quality Control), Budapest, Hungary, 2001. [online] Available at: https://njt.hu/jogszabaly/2001-201-20-22.34 [Accessed: 08 May 2025] (in Hungarian)